Current Profile Tracking for the DIII-D Tokamak via LQI Optimal Control

Mark D. Boyer, Justin Barton, Eugenio Schuster, Michael L. Walker,
Tim C. Luce, John R. Ferron, Ben G. Penaflor, Robert D. Johnson, and David A. Humphreys

***Abstract*— In tokamak fusion plasmas, controlling the spatial distribution profile of the toroidal current is key to achieving advanced scenarios characterized by confinement improvement and possible steady-state operation. The dynamics of the current profile are nonlinear and coupled with other plasma parameters, motivating the use of model-based control strategies. In this work, we use a control-oriented model of the current profile evolution in DIII-D to design a feedback controller for regulating the profile around a desired trajectory. Without feedback, the response of the current profile to disturbances, model uncertainty, and perturbed initial conditions can be undesirable. To improve tracking performance of the system, a nonlinear input transformation is combined with a linear-quadratic-integral (LQI) optimal controller designed to minimize a weighted combination of the tracking error and controller effort. The resulting control law utilizes the total plasma current, total external heating power, and line averaged plasma density as actuators. We present simulation and experimental results showing successful rejection of perturbed initial conditions and input disturbances.**

I. Introduction

When two light atomic nuclei react to form a heavier nucleus, a process called nuclear fusion, a portion of the mass is converted into energy. For the reaction rate to be high enough to make fusion energy an economical energy source, the fuel, typically deuterium and tritium, must be heated to extremely high temperatures. At these temperatures, the fuel becomes a plasma. The tokamak, which traps the ionized fuel particles with helical magnetic fields, is one of the most promising devices for confining a fusion plasma. The ITER tokamak, under construction in France, is the next step for fusion research and is designed to show the technical feasibility of a commercial nuclear fusion power plant. However, several challenging problems must be addressed before the promise of nuclear fusion energy can be realized.

A major challenge for tokamaks is achieving sufficiently long plasma discharges. Steady-state operation will require the plasma current to be driven by primarily non-inductive means, since plasma current driven purely through induction cannot be sustained for extended periods of time. It has been shown that the spatial distribution of toroidal plasma current plays an important part in enabling high fusion gain and non-inductive plasma current sustainment (see [1]). Modeling of the spatial distribution of toroidal current is generally simplified by assuming axisymmetry, reducing the problem of current current profile control to one-dimension. As part of the effort to identify and achieve suitable profiles for advanced operating scenarios, active control of the current profile or the safety factor profile, q, a related quantity (see definition below), has become an area of extensive research.

Most experiments in this area have used non-model-based real-time feedback approaches to control scalar parameters characterizing some aspect of the current profile. On DIII-D, feedback control of $q(0,t)$, the safety factor at the magnetic axis of the plasma, or $q_{min}(t)$, the minimum value of the safety factor profile, was achieved by modifying either ECH (electron cyclotron heating) or NBI (neutral beam injection) [2]. In [3], LHCD (lower hybrid current drive) was used to control the internal inductance parameter, $l_i(t)$, a measure of the current profile shape, on Tore Supra. Non-model based approaches were also studied in [4], [5], and [6].

Though non-model-based techniques have had some success in manipulating scalar outputs, like $l_i(t)$ or $q_{min}(t)$, it may be critical to control the shape of the entire current profile to achieve certain advanced tokamak operating scenarios. The strong nonlinear coupling between magnetic and kinetic profiles and the high dimensionality of this type of distributed control problem motivate the use of model-based techniques that can exploit the knowledge of the dynamic response of the system to the available actuators within the controller design. Compared to non-model-based approaches, model-based designs can achieve high levels of performance without requiring significant amounts of experimental time for trial-and-error tuning. Work on dynamic modeling of the current profile evolution has focused on either generating models from experimental data or creating models motivated by a first-principles description of the system.

A first-principles-driven dynamic model of the current profile evolution in DIII-D suitable for control design was developed in [7]. The current profile is related to the magnetic flux, which is modeled in normalized cylindrical coordinates by a parabolic partial differential equation (PDE) called the magnetic diffusion equation. Self-generated, non-inductive current sources were neglected in the derivation of the model, making the model appropriate for the inductively driven ramp-up and early flat-top phase of discharges or for the entirety of L-mode (low confinement) discharges in which the non-inductive source is typically small. In the model, the dynamics can be influenced through three different actuators: total plasma current, non-inductive heating/current-drive, and average plasma density. Nonlinear combinations of these actuators enable interior, boundary, and diffusivity control.

This work was supported by the National Science Foundation CAREER Award program (ECCS-0645086) and the U.S. Department of Energy (DE-FG02-09ER55064). M. D. Boyer (m.dan.boyer@lehigh.edu), J. Barton, and E. Schuster are with the Department of Mechanical Engineering and Mechanics, Lehigh University, Bethlehem, PA 18015, USA. M. L. Walker, T. C. Luce, J. R. Ferron, B. G. Penaflor, R. D. Johnson, and D. A. Humphreys are with General Atomics, San Diego, CA 92121, USA.

Utilizing this model, sets of optimal open-loop (feedforward) control trajectories have been designed based on nonlinear programming [8] and extremum seeking [9] approaches. This approach is limited in that the inputs are computed off-line and not modified in real-time to account for external disturbances, changes in the initial conditions, or modeling errors. To improve upon the performance and robustness properties of the system, we propose to add a feedback control law to the scheme. The nonlinear PDE model of the current profile evolution is first reduced through a nonlinear transformation of the physical inputs, discretization in space using a finite difference method, and linearization of the state dynamics. A linear quadratic integral optimal controller is then designed based on the reduced model. The presence of an integral term in the scheme improves upon the disturbance rejection and reference tracking performance of the closed loop system. Through nonlinear transformation of the resulting controller outputs, we obtain a feedback law for the plasma current, non-inductive heating power, and line averaged plasma density. The technique can be used to supplement any arbitrary feedforward trajectories, whether they are obtained through model-based optimization [8], [9] or determined experimentally. Numerical simulations of the scheme show improved closed loop performance and the results are confirmed in a series of experiments on DIII-D.

The paper is organized as follows. In Section II, a PDE model for the current profile evolution is introduced. The infinite dimensional model is reduced to a finite dimensional one in Section III and a set of the most relevant control channels is identified in Section IV. In Section V, a linear-quadratic-integral feedback control law is designed. Results of a simulation study are shown in Section VI and one of several experimental test cases is presented in Section VII. Conclusions and plans for future work are given in Section VIII.

II. Current Profile Evolution Model

We take ρ to be an arbitrary coordinate that indexes the magnetic flux surfaces within the tokamak plasma. Any quantity that is constant on each surface could be chosen as the indexing variable. Here we choose the mean geometric radius of the magnetic surface as ρ, i.e., $\pi B_{\phi,0}\rho^2 = \Phi$, where Φ is the toroidal magnetic flux and $B_{\phi,0}$ is the reference magnetic field at the geometric major radius R_0 of the tokamak. We normalize the quantity by the the mean geometric radius of the last closed magnetic surface, ρ_b, to obtain $\hat{\rho} = \rho/\rho_b$. The safety factor $q(\rho,t) = -d\Phi/d\Psi(\rho,t)$, where Ψ is the poloidal magnetic flux, is related to the toroidal current density. Noting the constant relationship between ρ and Φ, i.e., $\pi B_{\phi,0}\rho^2 = \Phi$, and the definition of ρ_b, the safety factor can be written as

$$q(\hat{\rho},t) = -\frac{B_{\phi,0}\rho_b^2\hat{\rho}}{\partial\psi/\partial\hat{\rho}}$$

where ψ is the poloidal stream function ($\Psi = 2\pi\psi$). To model the current profile dynamics, we therefore begin with the magnetic diffusion equation [7], [10]

$$\frac{\partial\psi}{\partial t} = \frac{\eta(T_e)}{\mu_0\rho_b^2\hat{F}^2}\frac{1}{\hat{\rho}}\frac{\partial}{\partial\hat{\rho}}\left(\hat{\rho}\hat{F}\hat{G}\hat{H}\frac{\partial\psi}{\partial\hat{\rho}}\right) + R_0\hat{H}\eta(T_e)\frac{<\bar{j}_{NI}\cdot\bar{B}>}{B_{\phi,0}} \tag{1}$$

where t is time, η is the plasma resistivity, which is dependent on the electron temperature T_e, μ_0 is the vacuum permeability, $\bar{j}_{NI}$ is the non-inductive current density (from neutral beam injection), $\bar{B}$ is the magnetic field, and $<>$ denotes the flux-surface average of a quantity. $\hat{F}$, $\hat{G}$, and $\hat{H}$ are spatially varying geometric factors of the DIII-D tokamak and are described in [7]. The boundary conditions are

$$\left.\frac{\partial\psi}{\partial\hat{\rho}}\right|_{\hat{\rho}=0} = 0 \qquad \left.\frac{\partial\psi}{\partial\hat{\rho}}\right|_{\hat{\rho}=1} = -\frac{\mu_0}{2\pi}\frac{R_0}{\hat{G}\Big|_{\hat{\rho}=1}\hat{H}\Big|_{\hat{\rho}=1}}I(t)$$

where $I(t)$ denotes the total plasma current. Simplified scenario-oriented models of the electron temperature, non-inductive current density, and resistivity, identified from experimental observations at DIII-D [7], are used to close the model. As the safety factor q inversely depends on the spatial derivative of the poloidal flux, we define

$$\theta(\hat{\rho},t) = \frac{\partial\psi}{\partial\hat{\rho}}(\hat{\rho},t) \tag{2}$$

and take this quantity as the to-be-controlled variable. This definition, along with the empirical correlations, allows us to write the control-oriented PDE governing θ as

$$\frac{\partial\theta}{\partial t} = h_0u_1\frac{\partial^2\theta}{\partial\hat{\rho}^2} + h_1u_1\frac{\partial\theta}{\partial\hat{\rho}} + h_2u_1\theta + h_3u_2 \tag{3}$$

where h_0, h_1, h_2, h_3 are spatially varying functions. The boundary conditions become

$$\theta\Big|_{\hat{\rho}=0} = 0 \qquad \theta\Big|_{\hat{\rho}=1} = -k_3u_3(t) \tag{4}$$

The equation admits diffusivity, interior, and boundary actuators u_1, u_2, and u_3, respectively, which each represent nonlinear combinations of the physical actuators, plasma current I, total beam heating power P_{tot}, and line averaged density $\bar{n}$. Note that the waveforms generated by the controller proposed in this work represent references to be sent to existing dedicated controllers for the respective quantities. The actuators are defined as

$$u_1(t) = \left(\frac{\bar{n}(t)}{I(t)\sqrt{P_{tot}(t)}}\right)^{3/2},\ u_2(t) = \frac{\sqrt{P_{tot}(t)}}{I(t)},\ u_3(t) = I(t) \tag{5}$$

III. Model Reduction via Spatial Discretization

In order to facilitate the controller design process, the governing PDE (3) is discretized into l nodes using a central difference formula for the $m = l-2$ interior nodes and forward/backward difference formulae for the left/right boundary nodes. By noting the boundary conditions (4), the resulting set of ODEs can be expressed as

$$\dot{\alpha}(t) = M\alpha(t)v_1(t) + Nv_2(t) + Zv_3(t) \tag{6}$$

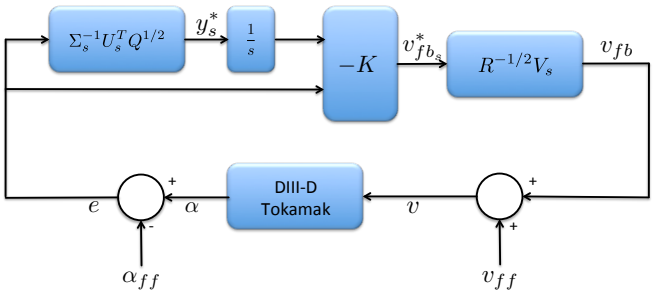

Fig. 1. LQI control scheme.

where $\alpha = [\theta_2, \ldots, \theta_{l-1}]^T \in \mathbb{R}^{m\times 1}$ is the value of $\theta(\hat{\rho}, t)$ at the interior nodes, the control input vectors are given by

$$[v_1(t), v_2(t), v_3(t)]^T = [u_1(t), u_2(t), u_1(t)u_3(t)]^T \in \mathbb{R}^{3\times 1}, \quad (7)$$

and $M \in \mathbb{R}^{m\times m}$, $N \in \mathbb{R}^{m\times 1}$, and $Z \in \mathbb{R}^{m\times 1}$.

We let $\alpha_{ff}(t)$ and $v_{ff}(t) = \left[v_{1_{ff}}(t), v_{2_{ff}}(t), v_{3_{ff}}(t)\right]$ represent a set of feedforward state and control trajectories, which are computed offline for a nominal initial state $\alpha_{ff}(0)$. The open-loop state trajectory satisfies

$$\dot{\alpha}_{ff}(t) = M\alpha_{ff}(t)v_{1_{ff}}(t) + Nv_{2_{ff}}(t) + Zv_{3_{ff}}(t) \quad (8)$$

Defining the fluctuation from the desired feedforward trajectory as $e(t) = \alpha(t) - \alpha_{ff}(t)$ and using $v_{fb}(t) = \left[v_{1_{fb}}(t), v_{2_{fb}}(t), v_{3_{fb}}(t)\right]$ as the to-be-designed feedback control inputs, allows us to write

$$\begin{aligned}\dot{\alpha}_{ff}(t) + \dot{e} = &M\alpha_{ff}\left(v_{1_{ff}} + v_{1_{fb}}\right) + Me\left(v_{1_{ff}} + v_{1_{fb}}\right) \\ &+ N\left(v_{2_{ff}} + v_{2_{fb}}\right) + Z\left(v_{3_{ff}} + v_{3_{fb}}\right) \quad (9)\end{aligned}$$

By substituting (8) in (9) we obtain a bilinear model. While we preserve the input nonlinearities by the nonlinear transformations (5) and (7), we approximately linearize the state dynamics by neglecting the bilinear term since $v_{1_{ff}} \gg v_{1_{fb}}$. Simulations and experiments show the closed loop system to be robust to this approximation. The dynamics of the error can then be expressed as the linear time-varying system

$$\dot{e} = A(t)e + B(t)v_{fb} \quad (10)$$

where $A(t) = Mv_{1_{ff}}(t) \in \mathbb{R}^{m\times m}$ and $B(t) = \left[M\alpha_{ff}(t), N, Z\right] \in \mathbb{R}^{m\times 3}$. We consider the case in which the states e are all measured, i.e, the output equation is $y = Ce + Dv_{fb}$ with $C = I$ and $D = 0$.

IV. Model Reduction via SVD

At this point a linear-quadratic-regulator (LQR) problem could be solved for the time-varying system (10), however, the resulting state feedback controller may not perform well in the presence of disturbances or during tracking experiments. To improve upon disturbance rejection and tracking, a feedback term proportional to the time integral of the states can be included in the control law, describing a linear-quadratic-integral (LQI) control problem. Since the system has multiple inputs and many outputs, such a design would create a high order controller. Additionally, since the system is underactuated, the resulting feedback algorithm could integrate states that are difficult to control, which could lead to controller wind-up and use of excessive amounts of control effort without achieving worthwhile improvement in system performance. To avoid this problem, we first decouple the system (10) at steady state through singular value decomposition (SVD) to reduce the underactuated, coupled system to a set of relevant control channels. We then keep only the most significant singular values, that is, the control channels through which the most influence on the system is realized, to further reduce the problem and avoid excessive controller effort.

After the ramp-up phase of the discharge, $v_{1_{ff}}$ and α_{ff} remain approximately constant, such that (10) can be reduced to a time invariant system

$$\dot{e} = \bar{A}e + \bar{B}v_{fb} \quad (11)$$

where $\bar{A} = A(t_f)$, $\bar{B} = B(t_f)$ and t_f is some time during the flat-top phase of the discharge. The transfer function of the system can then be expressed as $G(s) = C(sI - \bar{A})^{-1}\bar{B} + D$. By assuming closed-loop stability, we can write the steady-state ($s \to 0$) input-output relationship as $\bar{y} = \bar{G}\bar{v}_{fb} = -C\bar{A}^{-1}\bar{B}\bar{v}_{fb}$, where steady state values are denoted with an overbar. We then define the weighted steady-state transfer function

$$\tilde{G} = Q^{1/2}\bar{G}R^{-1/2} \quad (12)$$

where $Q \in \mathbb{R}^{m\times m}$ is a symmetric positive definite weighting matrix and $R \in \mathbb{R}^{3\times 3}$ is a positive definite weight matrix for the controller effort. The singular value decomposition of (12) is given by $\tilde{G} = U\Sigma V^T$ with $\Sigma = \mathrm{diag}(\sigma_1, \sigma_2, \sigma_3) \in \mathbb{R}^{3\times 3}$ and where $U \in \mathbb{R}^{m\times 3}$ and $V \in \mathbb{R}^{3\times 3}$ are unitary matrices. The steady-state input-output relation can then be expressed as

$$\bar{y} = Q^{-1/2}U\Sigma V^T R^{1/2}\bar{v}_{fb}$$

Since the columns of the matrix $Q^{-1/2}U\Sigma$ define a basis for the subspace of obtainable steady-state output values, we can write $\bar{y} = Q^{-1/2}U\Sigma\bar{y}^*$ where $\bar{y}^* \in \mathbb{R}^{3\times 1}$. By defining $\bar{v}_{fb}^* = V^T R^{1/2}\bar{v}_{fb}$, a one-to-one relationship between the inputs $\bar{v}_{fb}^*$ and the outputs $\bar{y}^*$, i.e.,

$$\bar{y}^* = \Sigma^{-1}U^T Q^{1/2}\bar{y} = \Sigma^{-1}U^T Q^{1/2}Q^{-1/2}U\Sigma V^T R^{1/2}\bar{v}_{fb} = \bar{v}_{fb}^* \quad (13)$$

For the model reduction, we consider the task of minimizing the steady-state performance index $\bar{J} = \lim_{t\to\infty} \bar{y}^T Q\bar{y} + \bar{v}_{fb}^T R\bar{v}_{fb}$. Since the system (13) is a square decoupled system, the performance index can be expressed as

$$\bar{J} = (\bar{y}^*)^T \Sigma^2 \bar{y}^* + \left(\bar{v}_{fb}^*\right)^T \Sigma^2 \bar{v}_{fb}^* = \sum_{i=1}^{3} \sigma_i^2 \left(\bar{y}_i^*\right)^2 + \sigma_i^2 \left(\bar{v}_{fb_i}^*\right)^2 \quad (14)$$

To avoid spending excessive control effort on realizing insignificant reductions in the performance index, we partition the singular values into s significant singular values Σ_s and n negligible singular values Σ_n. We then write

$$U = [U_s\, U_n] \quad V = [V_s\, V_n] \quad \Sigma = \begin{bmatrix} \Sigma_s & 0 \\ 0 & \Sigma_n \end{bmatrix}$$

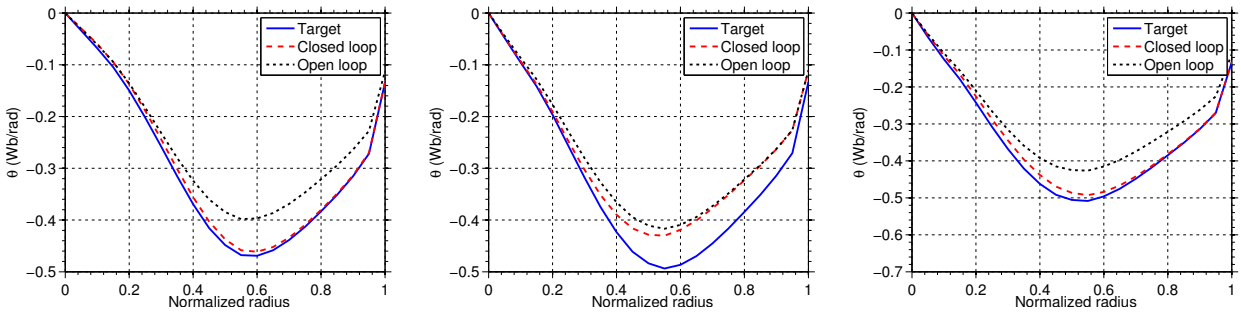

(a) $t = 2.50$s (b) $t = 3.50$s (c) $t = 5.00$s

Fig. 2. Comparison of θ profiles at various times for the target simulation (blue-solid), the open loop simulation (black - dash-dot), and the closed loop simulation (red-dashed). Progress towards the target profile is seen in (a), while the target is nearly achieved in (b). The effect of turning off the controller can be noted in (c).

$$\bar{y}^* = \begin{bmatrix} \bar{y}_s^* & \bar{y}_n^* \end{bmatrix}^T \quad \bar{v}_{fb}^* = \begin{bmatrix} \bar{v}_{fb_s}^* & \bar{v}_{fb_n}^* \end{bmatrix}^T$$

where

$$\begin{array}{ll} \bar{y}_s^* = \Sigma_s^{-1} U_s^T Q^{1/2} \bar{y} & \bar{v}_{fb_s}^* = V_s^T R^{1/2} \bar{v}_{fb} \\ \bar{y}_n^* = \Sigma_n^{-1} U_n^T Q^{1/2} \bar{y} & \bar{v}_{fb_n}^* = V_n^T R^{1/2} \bar{v}_{fb} \end{array} \Rightarrow \begin{array}{l} \bar{y} \approx Q^{-1/2} U_s \Sigma_s \bar{y}_s^* \\ \bar{v}_{fb} \approx R^{-1/2} V_s \bar{v}_{fb_s}^* \end{array}$$

We utilize the "significant" bases obtained through the steady-state analysis to approximate the cost function (14) as

$$\bar{J}_s = (\bar{y}_s^*)^T \Sigma_s^2 \bar{y}_s^* + \left(\bar{v_{fb_s}}^*\right)^T \Sigma_s^2 \bar{v_{fb_s}}^*$$

and the dynamic system (10) as

$$\begin{array}{rcl} \dot{e} & = & A_s(t)e + B_s(t)v_{fb_s}^* \\ y_s^* & = & C_s e + D_s v_{fb_s}^* \end{array}$$

where $A_s(t) = A(t)$, $B_s(t) = B(t)R^{-1/2}V_s$, $C_s = \Sigma_s^{-1}U_s^T Q^{1/2}$, $D_s = 0$. We then design a linear quadratic integral controller that uses the input $v_{fb_s}^*$ to drive the states e and the time integral of the significant output, y_s^*, to zero. The addition of the integral term gives the control scheme better disturbance rejection and reference tracking capabilities.

V. LQI Optimal Controller Design

To solve the LQI problem, we define an augmented state

$$x = \begin{bmatrix} \int_0^t y_s^* dt' \\ e \end{bmatrix}$$

to write a new, augmented system

$$\dot{x} = A_+(t)x + B_+(t)v_{fb_s}^*$$

where $A_+(t) = \begin{bmatrix} 0^{s\times s} & C_s \\ 0^{m\times s} & A_s(t) \end{bmatrix}$ and $B_+(t) = \begin{bmatrix} D_s \\ B_s(t) \end{bmatrix}$. We then proceed with a classic linear quadratic regulator design, i.e., we state the optimal control problem as

$$\min_{v_{fb_s}} J_+ = \frac{1}{2}\int_{t_0}^{\infty} \left[x^T Q_+ x + \left(v_{fb_s}^*\right)^T R_+ v_{fb_s}^*\right] dt$$

where $Q_+ \in \mathbb{R}^{m+s\times m+s}$ is symmetric positive semi-definite and R_+ is a positive scalar. The optimal control law is

$$v_{fb_s}^*(t) = -K(t)x(t)$$

where $K(t) \in \mathbb{R}^{s\times m+s}$ is given by $K = R_+^{-1}B_+^T(t)S_+(t)$ and $S_+(t)$ is the solution to the differential Riccati equation

$$\dot{S}_+ = -S_+A_+ - A_+^T S_+ + S_+ B_+ R_+^{-1} B_+^T S_+ - Q_+$$

subject to the condition $S_+(\infty) = 0$. The first s elements of $K(t)$ represent the integral gains, $K_I(t)$, while the remaining elements are state feedback gains K_P, i.e.,

$$v_{fb_s}^*(t) = -K_I(t)\int_0^t y_s^* dt' - K_P(t)e(t)$$

Noting the definitions of $v_{fb_s}^*$, y_s^*, and recalling $y = Ce = e$, we can write

$$v_{fb} = -R^{-\frac{1}{2}}V_s K_I(t)\int_0^t \left(\Sigma_s^{-1}U_s^T Q^{\frac{1}{2}} e\right) dt' - R^{-\frac{1}{2}}V_s K_P(t)e(t) \tag{15}$$

Finally, the controller can be put into state-space form

$$\begin{array}{rcl} \dot{x}_c & = & A_c x_c + B_c e \\ v_{fb} & = & C_c(t)x_c + D_c(t)e \end{array} \tag{16}$$

where x_c is the controller state representing the integral term in (15), $A_c = 0$, $B_c = \Sigma_s^{-1}U_s^T Q^{1/2}$, $C_c(t) = -R^{-1/2}V_s K_I(t)$, and $D_c(t) = -R^{-1/2}V_s K_P(t)$. Once v_{fb} is calculated, the values are added to the feedforward values v_{ff}. The resulting $v = v_{ff} + v_{fb}$ is put in terms of the physical actuators through the inverse of the nonlinear transformations (5) and (7), i.e.,

$$I_p = \frac{v_3}{v_1} \quad P_{tot} = \left(\frac{v_2 v_3}{v_1}\right)^2 \quad \bar{n} = \frac{v_2 v_3^2}{v_1^{4/3}}$$

The control scheme is illustrated in Figure 1. Because we have chosen an infinite time horizon for the optimal control problem and the system matrices A_+ and B_+ remain approximately time-invariant after the short ramp-up phase of the discharge, S_+ will be approximately a constant matrix $\bar{S}_+$ for most of the flat-top phase of the discharge. The matrix $\bar{S}_+$ can be obtained by solving the algebraic Riccati equation

$$0 = -\bar{S}_+A_+(t_f) - A_+^T(t_f)\bar{S}_+ + \bar{S}_+B_+(t_f)R_+^{-1}B_+^T(t_f)\bar{S}_+ - Q_+$$

where t_f is a time during the flat-top phase. The controller gain is then reduced to a constant $\bar{K} = R_+^{-1}B_+^T(t_f)\bar{S}_+$ and the system (16) becomes LTI. In the simulation and experimental results shown in the following sections, we utilize the LTI approximation of the optimal control law and keep just one singular value.

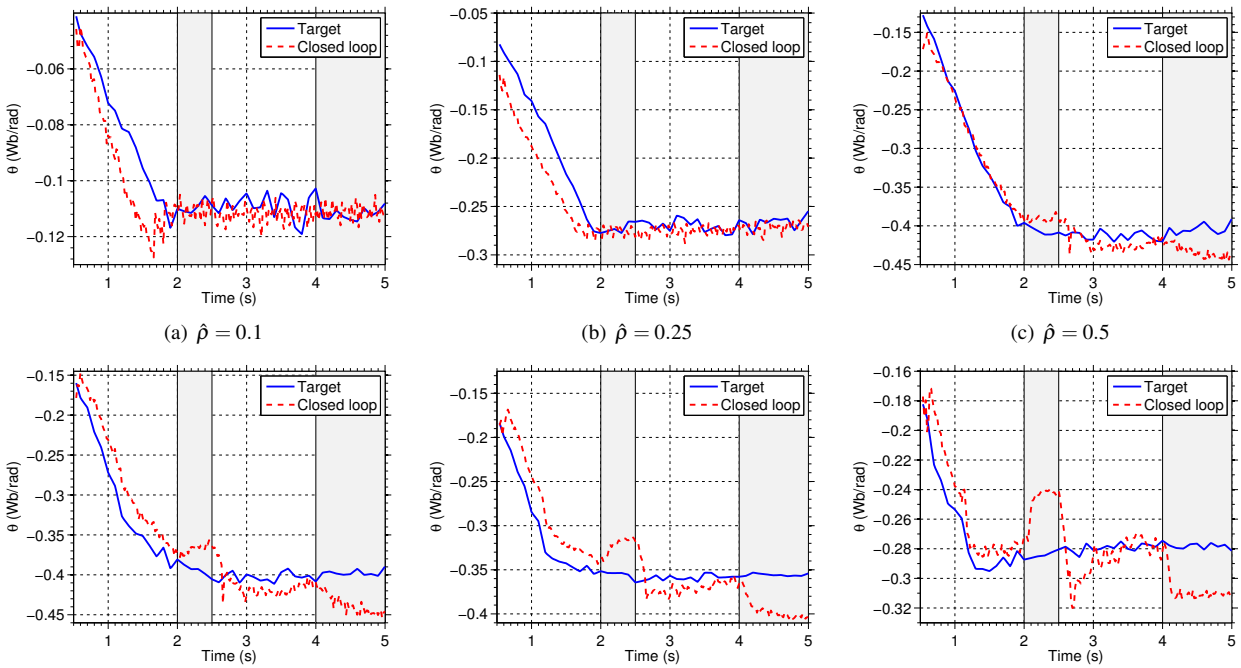

(a) $\hat{\rho} = 0.1$ (b) $\hat{\rho} = 0.25$ (c) $\hat{\rho} = 0.5$

(d) $\hat{\rho} = 0.65$ (e) $\hat{\rho} = 0.8$ (f) $\hat{\rho} = 0.95$

Fig. 3. Time trace of θ at various points comparing the reference shot 145477 (blue-solid) and the closed loop, disturbed shot 146414 (red-dashed) Feedback was turned off in the shaded regions of the plot.

VI. Simulation Results

Prior to experimental testing of the control scheme, a simulation study was performed to test and tune the controller. To test the reference tracking ability of the controller, we used a particular set of feedforward inputs to generate a θ profile evolution, which we took as the target profile for subsequent simulations. A different set of feedforward inputs (inconsistent with the target) were used in two shots: one without feedback (open loop) and one with feedback (closed loop). During the closed loop shot, the controller was turned on from 0.5s to 2.5s to test performance, then turned off from 2.5s to 3.5s to observe the uncontrolled evolution. From 3.5s to the end of the simulation, the controller was turned back on to see if it could recover the desired target profile.

In Figure 2, the profiles achieved in the closed loop shot and the open loop shot are compared with the target profile at several times. Figure 2(a) shows that the closed loop system has nearly achieved the desired profile by $t = 2.5$s. Figure 2(b) shows the increased error caused by the uncontrolled drift phase ($t = 2.5s$ to $t = 3.5s$). Recovery of the desired profile after the controller is turned back on is clear in Figure 2(c).

VII. Experimental Results

In this section, we present results from an experimental test on the DIII-D tokamak. First, an open loop (feedforward only) discharge (DIII-D shot 145477) was performed. The resulting θ profile evolution was then used as the target for the closed loop (feedforward+feedback) shot 146414.

For shot 146414, an artificial input disturbance of -0.15 MA in the plasma current and -0.5 MW in the total non-inductive power was added to the reference inputs (taken from 145477) from $t = 0.5$s to $t = 2.5$s. The feedback controller was turned on from $t = 0.5$s to $t = 2.0$s to test disturbance rejection and switched off from $t = 2.0$s to $t = 2.5$s to see the influence of the input disturbance. At $t = 2.5$s the disturbance was changed to 0.15 MA in the plasma current and 0.5 MW in the heating power and the controller was turned back on to see if the controller could recover the desired profile despite the error caused by the drift and the presence of the new disturbance. At $t = 4.0$s, the controller was switched off to observe the effect of the uncontrolled disturbance.

Time traces of θ at several points along the profile are given in Figure 3. The results of the closed loop shot 146414 are compared with the target generated in shot 145477. The controller successfully rejects the disturbance during the first phase ($t = 0.5$s to $t = 2.0$s) and the error caused by the uncontrolled disturbance is clear during the drift phase ($t = 2.0$s to $t = 2.5$s). When the disturbance is changed and the controller is turned back on at $t = 2.5$s, the target values of θ are quickly recovered. Finally, the uncontrolled response of the system to the second disturbance is evident after $t = 4.0s$. In Figure 4, the profiles achieved in the closed loop, disturbed shot 146414 are compared with the desired reference profiles obtained from shot 145477 at several times. Figure 4(a) shows that the controller has nearly recovered the desired profile shortly before it is turned off at $t = 2.0$s. Figure 4(b) shows the error resulting from the disturbance after the uncontrolled drift phase ($t = 2.0s$ to $t = 2.5s$) and the successful recovery of the desired profile after the controller is turned back on for a short time is clear in Figure 4(c). The

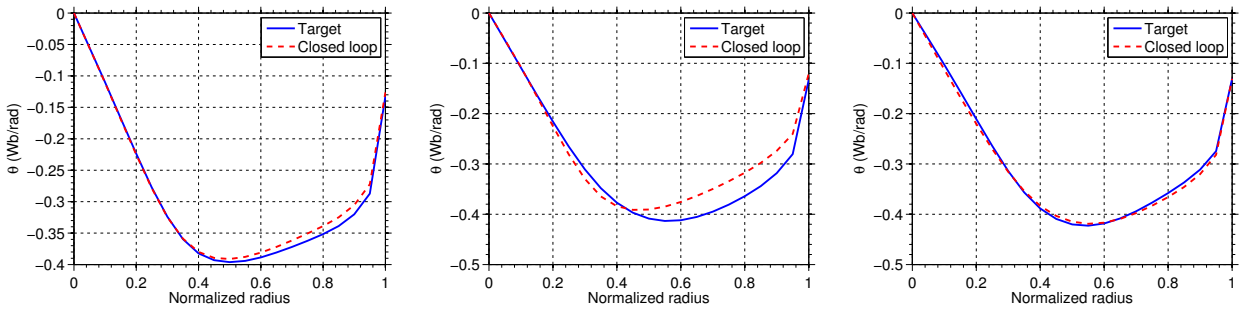

(a) $t = 2.00$s (Feedback on) (b) $t = 2.5$s (Feedback off) (c) $t = 4.00$s (Feedback on)

Fig. 4. Comparison of θ profiles at various times for reference shot 145477 (blue-solid) and the closed loop, disturbed shot 146414 (red-dashed). Successful disturbance rejection is seen in (a), while the effect of the uncontrolled disturbance can be noted in (b). Recovery of the target profile after the second disturbance is applied and the controller is turned back on can be observed in (c).

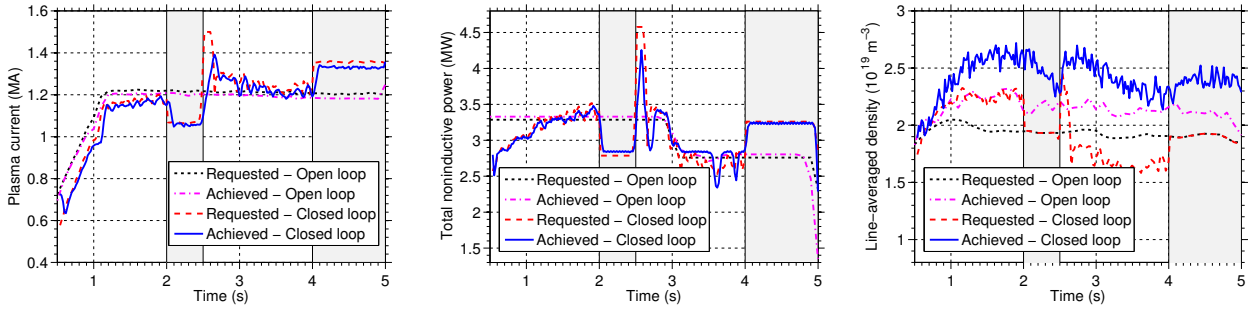

(a) Plasma current I_p (b) Total non-inductive power P_{tot} (c) Line averaged density $\bar{n}$

Fig. 5. Comparison of requested and achieved actuator values during the feedforward shot 145477 and the closed loop, disturbed shot 146414. Feedback control was turned off in the shaded regions of the plots.

actuator requests and achieved values are compared in Figure 5. It should be noted that while the total plasma current and total power are tightly controlled and the requests are reproduced quite well, the request for line averaged density is often not achieved. This represents an additional input disturbance aside from the intentional one added to test the controller.

VIII. Conclusions

We have presented a model-based current profile controller design for the DIII-D tokamak. The feedback controller was designed to compliment any arbitrary set of feedforward inputs and drive the spatial profile of the variable θ to the desired target profile. Through discretization of the original model, a finite dimensional, time-varying model for the profile error was obtained. A singular-value decomposition technique was then utilized to reduce the multi-input multi-output coupled system to a set of the most relavant control channels and a linear-quadratic-integral controller was then designed for the reduced order model. Through a nonlinear transformation, the resulting feedback control law outputs reference values for the total plasma current, non-inductive power, and plasma density. Both a simulation study and a successful experimental result are presented.

Performance improvement could potentially be achieved by keeping more than one singular value during the model reduction process, which would give the controller more degrees of freedom, or by implementing the time-varying optimal control law instead of the LTI approximation used here. In the future, we will extend the model to H-mode (high confinement mode) discharges for which the self-generated non-inductive current source neglected by the model used in this work becomes significant and must be accounted for.

References

[1] M. Murakami, M. R. Wade, C. M. Greenfield, *et al.*, "Progress toward fully noninductive, high beta conditions in DIII-D," *Phys. of Plasmas*, vol. 13, no. 5, p. 056106, 2006.

[2] J. Ferron, P. Gohil, C. Greenfield, *et al.*, "Feedback control of the safety factor profile evolution during formation of an advanced tokamak discharge," *Nuclear Fusion*, vol. 46, pp. L13–L17, Oct. 2006.

[3] T. Wijnands, D. V. Houtte, G. Martin, X. Litaudon, and P. Froissard, "Feedback control of the current profile on Tore Supra," *Nuclear Fusion*, vol. 37, pp. 777–791, June 1997.

[4] O. Barana, D. Mazon, L. Laborde, and F. Turco, "Feedback control of the lower hybrid power deposition profile on Tore Supra," *Plasma Phys. and Control. Fusion*, vol. 49, pp. 947–967, July 2007.

[5] T. Suzuki, "Recent RF experiments and application of RF waves to real-time control of safety factor profile in JT-60U," in *AIP Conference Proceedings*, vol. 787, pp. 279–286, 2005.

[6] T. Suzuki, S. Ide, T. Oikawa, T. Fujita, M. Ishikawa, M. Seki, G. Matsunaga, T. Hatae, O. Naito, K. Hamamatsu, M. Sueoka, H. Hosoyama, and M. Nakazato, "Off-axis current drive and real-time control of current profile in JT-60U," *Nucl. Fusion*, vol. 48, p. 045002, Apr. 2008.

[7] Y. Ou, T. Luce, E. Schuster, *et al.*, "Towards model-based current profile control at DIII-D," *Fusion Eng. and Design*, vol. 82, pp. 1153–1160, Oct. 2007.

[8] C. Xu, Y. Ou, J. Dalessio, *et al.*, "Ramp-up-phase current-profile control of tokamak plasmas via nonlinear programming," *IEEE Trans. on Plasma Sci.*, vol. 38, pp. 163–173, Feb. 2010.

[9] Y. Ou, C. Xu, E. Schuster, *et al.*, "Design and simulation of extremum-seeking open-loop optimal control of current profile in the DIII-D tokamak," *Plasma Phys. and Control. Fusion*, vol. 50, Nov. 2008.

[10] J. Blum, *Numerical simulation and optimal control in plasma physics: with applications to tokamaks*. John Wiley & Songs, 1989.